

Crystal structure and EPR of the $\text{RbNd}(\text{WO}_4)_2$ single crystal

M.T. Borowiec^{a,*}, A.D. Prokhorov^{a,b}, I.M. Krygin^b, V.P. Dyakonov^{a,b}, K. Woźniak^c,
Ł. Dobrzycki^c, T. Zayarnyuk^a, M. Barański^a, W. Domuchowski^a, H. Szymczak^a

^a*Institute of Physics, Polish Academy of Sciences, al. Lotników 32/46, 02 668 Warszawa, Poland*

^b*A. A. Galkin Donetsk Physic-Technical Institute, ul. Luxemburg 72 83114 Donetsk, Ukraine*

^c*Chemistry Department, Warsaw University, ul. Pasteura 1, 02 093 Warszawa, Poland*

Received 30 December 2004; received in revised form 30 August 2005; accepted 4 October 2005

Abstract

Crystal structure and EPR spectra in a $\text{RbNd}(\text{WO}_4)_2$ single crystal have been studied. $\text{RbNd}(\text{WO}_4)_2$ crystallizes in the monoclinic structure with the unit cell parameters: $a = 10.792(2) \text{ \AA}$, $b = 10.673(2) \text{ \AA}$, $c = 7.6703(15) \text{ \AA}$, $\beta = 130.51(3)^\circ$. Using the X-ray diffraction measurements, the fractional atomic coordinates, displacement parameters and interatomic distances have been determined. The EPR spectra are described in terms of the main \mathbf{g} -tensor values: $g_z = 3.291 \pm 0.005$, $g_x = 0.726 \pm 0.005$, $g_y = 1.533 \pm 0.005$. Both the magnetic dipole–dipole and isotropic exchange interactions have been calculated. The exchange interactions are shown to exceed the magnetic dipole–dipole interactions and to have an opposite sign. These results suggest an appearance of an antiferromagnetic ordering in $\text{RbNd}(\text{WO}_4)_2$ at low temperatures.

© 2005 Elsevier B.V. All rights reserved.

PACS: 61.66.–f; 76.30.–v

Keywords: Crystal structure; EPR spectra; \mathbf{g} tensor; Exchange and magnetic dipole–dipole interactions

1. Introduction

Over the past years, the family of rare-earth double tungstates with monoclinic symmetry has attracted significant interest. Such crystals can be used as active elements for excitation of laser action [1] and they show in addition an unusual physical properties at low temperatures [2,3]. In these crystals, paramagnetic ions are forming chains along one of the crystallographic axis. This results in both peculiarities of spin–spin interactions and an unusual shape of EPR spectrum, for example, as observed in $\text{KDy}(\text{WO}_4)_2$ [4]. Because of large g_z value of the Dy^{3+} ions, equal to 14.6, the EPR spectrum is observed at low fields. This does not allow to observe a full absorption line because of its large line width. According to Ref. [5], the g_z value of the Nd^{3+} ions introduced to $\text{KY}(\text{WO}_4)_2$ is equal of about 3, therefore, the replacement of Y^{3+} for Nd^{3+}

should allow to observe and analyze the EPR line in fields of about 2 kGs. However, the $\text{KNd}(\text{WO}_4)_2$ single crystals belong to the tetragonal syngony and have the structure different from that of $\alpha\text{-KY}(\text{WO}_4)_2$. Therefore, it was of interest to grow the $\text{RbNd}(\text{WO}_4)_2$ single crystals having the monoclinic symmetry and to study both their crystal structure and peculiarities of the EPR spectrum of Nd^{3+} ions.

2. Experimental

The single crystals of the potassium rare-earth double tungstate $\text{KRE}(\text{WO}_4)_2$ ($\text{RE} = \text{Gd} \dots \text{Lu}$ and also Y) belong to the centrosymmetric $2/m$ Laue class of the monoclinic system. The crystallographic structure of double tungstates has been studied in Refs. [6–10].

The double tungstate $\text{RbNd}(\text{WO}_4)_2$ undergoes the irreversible structural phase transition (SPT) at temperatures slightly below its melting points. To lower the temperature of crystallization below SPT, high temperature

*Corresponding author. Tel.: +48 22 8436601x3362.

E-mail addresses: borow@ifpan.edu.pl (M.T. Borowiec),
zayar@ifpan.edu.pl (T. Zayarnyuk).

solution growth (HTSG) technique was used. The RbNd(WO₄)₂ single crystals were grown by the top seeded solution growth (TSSG) technique using oriented RbNd(WO₄)₂ seeds obtained by the method of spontaneous crystallization in K₂W₂O₇ as solvent with slowly decreasing temperature.

The density of crystals is equal to 7.17 g/cm³. The violet color of single crystals is connected with optical absorption of neodymium ions. The energy gap is of about 3.8 eV.

X-ray structural investigations of powdered RbNd(WO₄)₂ were performed using a D-5000 Siemens type diffractometer with CuK_α radiation at the room temperature.

Diffractional measurements of the prismatic RbNd(WO₄)₂ single crystal (dimensions: 0.26 × 0.17 × 0.09 mm³) were performed using a Kuma KM4CCD four-circle κ-axis diffractometer with graphite-monochromatic MoK_α radiation, in which an omega scan technique was applied. The crystal was positioned at 65 mm from the KM4CCD camera. The collection of data was obtained with reduced accelerating voltage to 34.2 kV to eliminate evident “λ/2 contamination” effect [11]. The data were corrected taking into account the Lorentz and polarization effects. Analytical absorption correction was applied using the shape optimization procedure based on reflections, which are higher than their error by a factor 20. The data analysis was carried out using the Kuma diffraction suit of programs.

The unit cell parameters obtained were based on 10,000 reflections in the 2θ range from 8° to 100° with 1° intervals, while the structure was based on reflections under change of 2θ–70°.

The structure was solved by both the direct method [12] and refined one using SHELXL [13]. The refinement was based on F² for all reflections except those with very negative F². Scattering factors were taken from Tables 6.1.1.4 and 4.2.4.2 in Ref. [14].

For EPR investigations, the RbNd(WO₄)₂ single crystal was cut in the form of parallelepiped with orientation established by the X-ray diffraction method.

The EPR spectra studies were carried out in an X-band spectrometer with high-frequency modulation. The magnetic field was changed from 0 to 1 T. The EPR spectra measurements were performed over a temperature range from 4.2 to 300 K with use of the EPR Oxford Instrument ESR9 continuous flow cryostat. The rotation of sample in the various planes with angle accuracy of 1° was carried out using the goniometer.

3. Crystal structure

For the RbNd(WO₄)₂ powder, we have obtained the following unit cell parameters: $a = 10.7832(5) \text{ \AA}$, $b = 10.6363(1) \text{ \AA}$, $c = 7.6527(6) \text{ \AA}$, $\beta = 130.453(1)^\circ$, which are in good agreement with results obtained for the single crystal.

The crystal structure data together with the refinement details obtained for the RbNd(WO₄)₂ single crystal are given in Table 1. Fractional atomic coordinates, anisotropic displacement parameters and selected interatomic parameters are given in Tables 2–4, respectively.

For the RbNd(WO₄)₂ single crystals, we have obtained the following unit-cell parameters (Table 1): $a = 10.792(2) \text{ \AA}$, $b = 10.673(2) \text{ \AA}$, $c = 7.6703(15) \text{ \AA}$, $\beta = 130.51(3)^\circ$, with $Z = 4$ and the monoclinic space group C2/c.

According to Table 2, Rb and Nd ions occupy special positions 4e according to Wyckoff notation in C2/c space group. The local symmetry of these ions is C₂ in the

Table 1
Crystal structure data and refinement details

Empirical formula	NdRbO ₈ W ₂
Formula weight	725.41
Temperature	293(2) K
Wavelength	0.71073 Å
Crystal system, space group	Monoclinic, C2/c
Unit cell parameters	$a = 10.792(2) \text{ \AA}$ $\alpha = 90^\circ$ $b = 10.673(2) \text{ \AA}$ $\beta = 130.51(3)^\circ$ $c = 7.6703(15) \text{ \AA}$ $\gamma = 90^\circ$
Volume	671.7(2) Å ³
Z, Calculated density	4, 7.173 g cm ⁻³
Absorption coefficient	48.985 mm ⁻¹
F(000)	1236
Crystal size	0.26 × 0.17 × 0.09 mm
Theta range for data collection	3.82–34.99°
Limiting indices	$-17 < h < 17$, $-16 < k < 16$, $-12 < l < 12$
Reflections collected/unique	7472/1453 [$R(\text{int}) = 0.0613$]
Completeness to theta = 32.49	97.9%
Absorption correction	Analytical
Transmissions factors	$T_{\text{min}} = 0.07707$ $T_{\text{max}} = 0.00359$
Refinement method	Full-matrix least-squares on F ²
Data/restraints/parameters	1453/0/57
Goodness-of-fit on F ²	1.145
Final R indices [$I > 2\sigma(I)$]	$R1 = 0.0254$, $wR2 = 0.0740$ for 1390 reflections
R indices (all data)	$R1 = 0.0272$, $wR2 = 0.0752$
Extinction coefficient	0.00167(12)
Largest diff. peak and hole	2.063 and $-2.922 \text{ e \AA}^{-3}$

Table 2
Fractional atomic coordinates and equivalent isotropic displacement parameters (Å²...10³)

	Wyckoff position	x	y	z	U(eq)
Nd(1)	4e	1.0000	0.7725(1)	0.7500	7(1)
W(1)	8f	0.8079(1)	0.5014(1)	0.7680(1)	6(1)
Rb(1)	4e	1.0000	0.8022(1)	0.2500	14(1)
O(1)	8f	0.9756(4)	0.3943(3)	1.0261(6)	9(1)
O(2)	8f	0.8141(4)	0.4295(3)	0.5641(6)	11(1)
O(3)	8f	0.6325(4)	0.4253(4)	0.6940(6)	12(1)
O(4)	8f	0.7314(4)	0.6568(3)	0.6363(6)	12(1)

Table 3
Selected interatomic distances (Å) for RbNd(WO₄)₂

Nd(1)–O(1)#1	2.367(3)	W(1)–O(2)#9	2.347(3)
Nd(1)–O(1)#2	2.367(3)	Rb(1)–O(2)#1	2.908(4)
Nd(1)–O(3)#3	2.385(4)	Rb(1)–O(2)#11	2.908(4)
Nd(1)–O(3)#4	2.385(4)	Rb(1)–O(2)#3	2.921(4)
Nd(1)–O(4)#5	2.444(4)	Rb(1)–O(2)#12	2.921(4)
Nd(1)–O(4)#6	2.444(4)	Rb(1)–O(3)#3	3.007(4)
Nd(1)–O(4)	2.721(4)	Rb(1)–O(3)#12	3.007(4)
Nd(1)–O(4)#7	2.721(4)	Rb(1)–O(1)#11	3.111(3)
W(1)–O(2)	1.782(3)	Rb(1)–O(1)#1	3.111(3)
W(1)–O(3)	1.781(3)	Rb(1)–O(4)#13	3.165(4)
W(1)–O(4)	1.836(3)	Rb(1)–O(4)#6	3.165(4)
W(1)–O(1)	1.961(3)	Rb(1)–O(3)#13	3.389(4)
W(1)–O(1)#2	2.097(3)	Rb(1)–O(3)#6	3.389(4)

Symmetry transformations used to generate equivalent atoms: #1 $x, -y+1, z-1/2$; #2 $-x+2, -y+1, -z+2$; #3 $x+1/2, y+1/2, z$; #4 $-x+3/2, y+1/2, -z+3/2$; #5 $x+1/2, -y+3/2, z+1/2$; #6 $-x+3/2, -y+3/2, -z+1$; #7 $-x+2, y, -z+3/2$; #8 $x, y, z+1$; #9 $x, -y+1, z+1/2$; #10 $x-1/2, y-1/2, z$; #11 $-x+2, -y+1, -z+1$; #12 $-x+3/2, y+1/2, -z+1/2$; #13 $x+1/2, -y+3/2, z-1/2$.

Table 4
Anisotropic displacement parameters (ADP) (Å²...10³)

	U(11)	U(22)	U(33)	U(23)	U(13)	U(12)
Nd(1)	8(1)	5(1)	8(1)	0	5(1)	0
W(1)	6(1)	5(1)	7(1)	1(1)	4(1)	0(1)
Rb(1)	13(1)	15(1)	13(1)	0	8(1)	0
O(1)	9(1)	4(1)	12(1)	0(1)	6(1)	-1(1)
O(2)	13(1)	8(2)	12(1)	1(1)	9(1)	0(1)
O(3)	10(1)	13(2)	13(1)	1(1)	7(1)	-2(1)
O(4)	12(1)	5(1)	11(1)	3(1)	6(1)	1(1)

Schoenflies notation. The W1 cation occupies a general position, although its y coordinate is very close to $\frac{1}{2}$. This location influences thermal motions (Table 3) of this atom—the off-diagonal anisotropic displacement parameters (ADP) are almost equal to zero, within the experimental error (see U(23) and U(12) in Table 4).

The coordination figures of W, Nd and Rb cations are shown in Figs. 1–3. There are three kinds of polyhedrons in the RbNd(WO₄)₂ structure depending on the central cation. These are octahedron, dodecahedron and icosahedron around W, Nd and Rb ions, respectively (Fig. 3). Because of the low symmetry of this structure, each polyhedron is distorted. For the tungstate unit, there are three short distances W–O (ca. 1.8 Å), two distances close to 2 Å and one longer than 2.3 Å. So the octahedron is elongated in one direction. The distances between both neodymium and oxygen ions and Rb and O change from 2.37 to 2.72 Å and from 2.91 to 3.39 Å, respectively. Nd–O and Rb–O polyhedrons form chains along the $a+c$ axes, whereas the tungstate octahedrons compose the layers perpendicular to the b direction (Fig. 1).

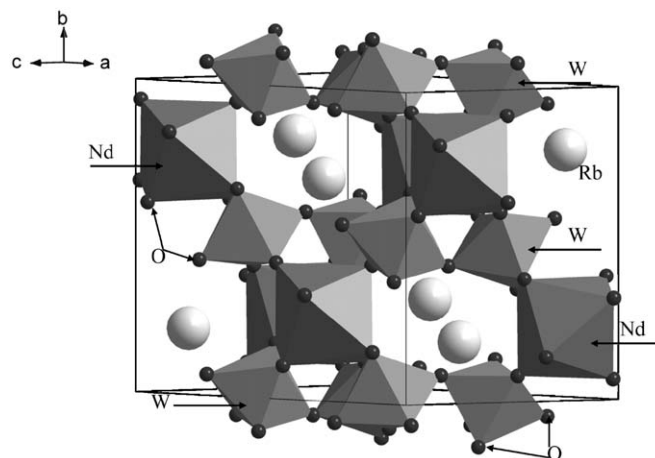


Fig. 1. The unit cell with W and Nd polyhedrons.

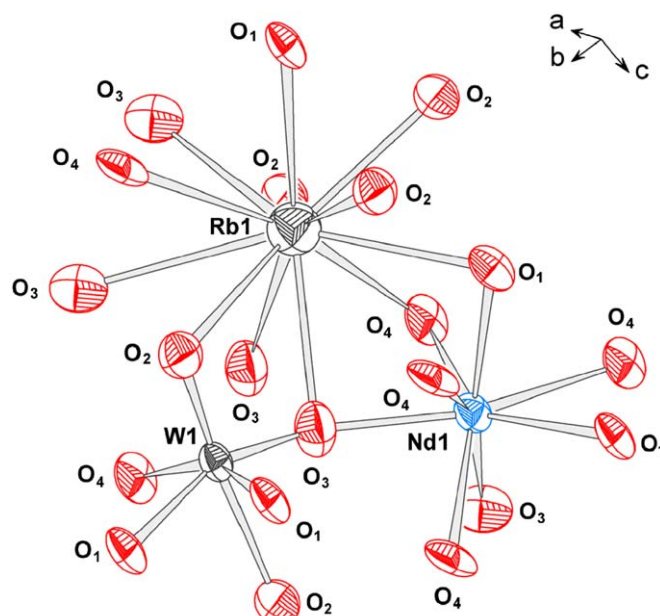


Fig. 2. Thermal ellipsoids with probability factor equal to 99%.

4. Angular dependence of the Nd³⁺ EPR spectrum

The electronic configuration of the trivalent neodymium ion is 4f³. The ground multiplet ⁴I_{9/2} is split by a double tungstate crystal field into five Kramers doublets, on the lowest of which microwave absorption is observed. According to the measurements of the angular dependence of the EPR spectrum in various crystalline planes two main axes of the g -tensor ($g_{\max} = g_z$ and $g_{\min} = g_x$) were established to lie in the ac plane. The third main axis of the g -tensor is parallel to the second-order axis C_2 and coincides with the crystallographic b -axis perpendicular to ac plane. The EPR spectrum represents the superposition of three lines of different intensity and width. The angular dependence of the central line of the spectrum in the ac plane is presented in Fig. 4 and it allows to find the

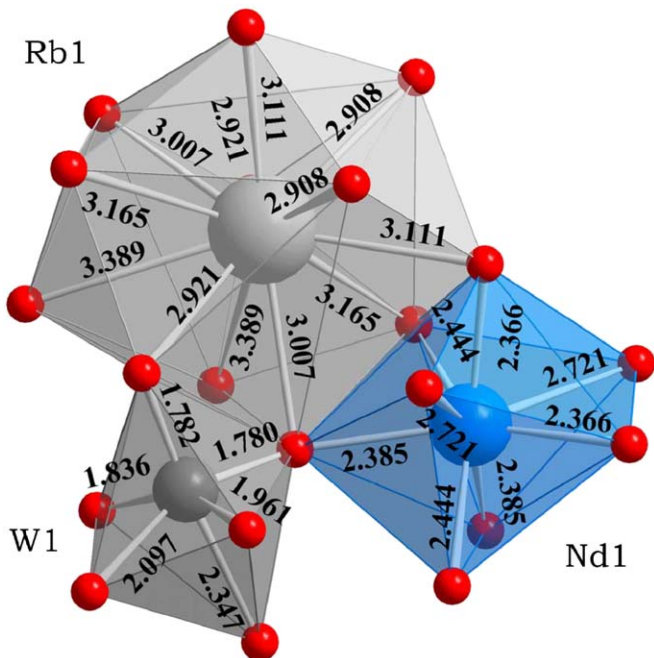


Fig. 3. Nd, Rb and W polyhedra with marked distances to ligands.

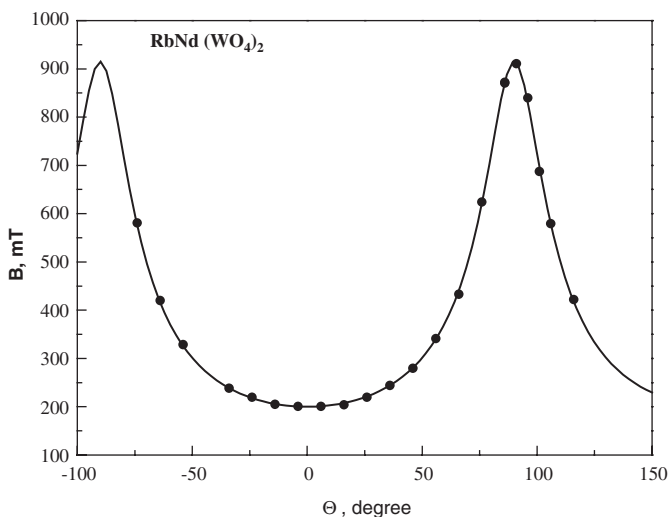


Fig. 4. The angular dependence of central line of EPR spectrum for the $\text{RbNd}(\text{WO}_4)_2$ single crystal in the ac plane (the points are experimental data, the solid line is the fitting curve obtained using the Hamiltonian (1)).

directions of g_{\max} and g_{\min} (the main axes z and x ; the z -axis is perpendicular to the x -axis). The line positions in magnetic field are strongly anisotropic and can be described by spin-Hamiltonian with the effective spin $S = \frac{1}{2}$

$$\hat{H} = \mu_B \mathbf{B} \mathbf{g} \hat{S}, \quad (1)$$

where μ_B is the Bohr magneton, \hat{S} the spin operator, \mathbf{g} the \mathbf{g} -tensor of the spectroscopic splitting, \mathbf{B} the induction of external magnetic field. The main values of \mathbf{g} -tensor are: $g_z = 3.291 \pm 0.005$, $g_x = 0.726 \pm 0.005$, $g_y = 1.533 \pm 0.005$. The g_{\min} direction (x -axis) has a deviation of about 5° from the crystallographic c -axis.

In accordance with crystallographic data, the nearest rare-earth ions are located in chains directed along the $a+c$ direction. As it follows from elementary geometrical calculations, the angle, which the z -axis forms with a chain formed by the rare-earth ions is of about 9.6° . The determination of this angle is important for the estimation of the spin–spin interaction between the neodymium ions.

5. The shape and width of EPR line

Fig. 5 presents the derivatives of the absorption line for various temperatures at $\mathbf{B} \parallel z$. The absorption spectrum observed has several peculiarities. At low temperatures ($T < 15$ K), the spectrum consists of the three lines of different intensities. The spectrum becomes asymmetrical with decreasing temperature, namely, the intensity of low-field line is smaller than the intensity of high-field one. The increase of the temperature causes a broadening of the lines, the fine structure of spectrum disappears, and as a result, a single wide symmetric line is observed. The further increase of the temperature above 50 K causes so strong broadening of single line that it becomes not observable. The temperature broadening is attributed to the strong spin–phonon interaction, which is characteristic of the unquenched orbital momentum systems (the rare-earth ions excluding the Gd^{3+} ions).

In oxide crystals, in the case of a low concentration of paramagnetic ions, the EPR line width usually does not exceed several Gs. As the EPR line width of $\text{K}(\text{Y} + 0.1\% \text{Dy}^{3+})(\text{WO}_4)_2$ is 0.7 mT, the hyperfine structure of spectrum is distinctly observed [15]. In the case of low concentration of the Nd^{3+} ions, a similar structure should be observed because the neodymium nuclei have an odd isotopes with nuclear spin of $I = 7/2$ ($^{143}\text{Nd} = 12.7\%$,

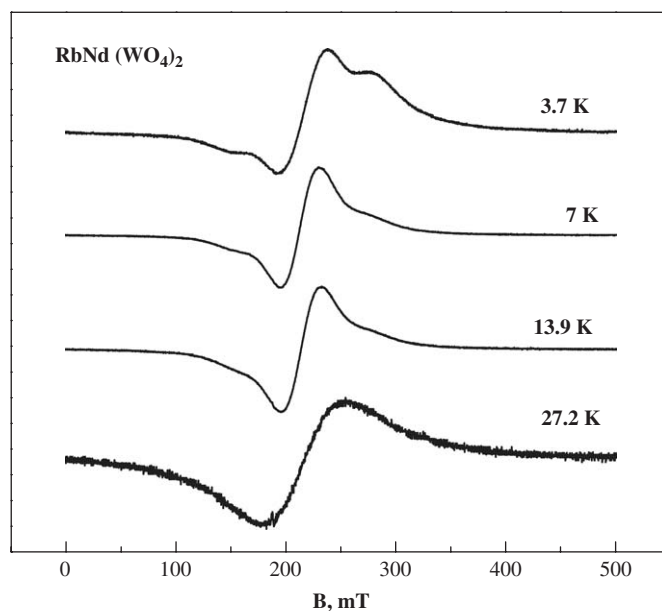


Fig. 5. The experimental EPR spectrum for the $\text{RbNd}(\text{WO}_4)_2$ single crystal for $\mathbf{B} \parallel z$ as a function of temperature.

$^{145}\text{Nd} = 8.3\%$). The greatest contribution to the absorption intensity is expected to be given by the nuclei with even isotopes. The increase of neodymium concentration leads to an increase of the contribution of spin–spin interactions (SSI) to the line widths, and as a result the diminishing of the hyperfine structure is observed.

The analysis of the EPR spectrum of Dy^{3+} ion pairs in $\text{KY}(\text{WO}_4)_2$ [16] has shown that the nearest ions located along the chains have the highest energy of interaction, approximately one order of magnitude, as compared with far removed ions.

Two simplifying assumptions were made to estimate the magnitude of SSI:

- (1) The interaction occurs only along the Nd^{3+} ions chain. In this case, the Hamiltonian describing the EPR spectrum of Nd^{3+} ions in $\text{RbNd}(\text{WO}_4)_2$ can be presented as a sum of contributions from all ions in the chain:

$$\hat{H} = \mu\mathbf{B}\mathbf{g} \sum \hat{\mathbf{S}}_i + \sum \hat{\mathbf{S}}_i \mathbf{K} \hat{\mathbf{S}}_{i+1}, \quad (2)$$

where the first term is the Zeeman interaction, the second one is the spin–spin interaction, $\hat{\mathbf{S}}_i$ is the spin operator of i th ion in the chain and \mathbf{K} is the tensor of the spin–spin interaction.

- (2) K_{zz} is the most important component of the \mathbf{K} -tensor, and it is confirmed by the fact that g_z is greater than g_x and g_y . In this case, the calculated EPR spectrum of the chain becomes considerably simpler and consists of only three components [17]. In our experiments, we have observed the similar picture. The distance between the extreme lines in experimentally found triplet is equal to $2K_{zz}$ (Fig. 5), where $K_{zz} = +728 \times 10^{-4} \text{ cm}^{-1}$. The sign of K_{zz} is determined by the ratio of intensities of the low- and high-field lines of the triplet.

The basic mechanisms determining the \mathbf{K} -tensor are a magnetic dipole–dipole interaction (MDD) and an isotropic exchange interaction (Ex):

$$\mathbf{K} = \mathbf{K}^{\text{MDD}} + \mathbf{K}^{\text{Ex}}. \quad (3)$$

The contribution of these mechanisms into \mathbf{K} is quadratic in g [18]:

$$K_{pq}^{\text{MDD}} = \frac{\mu^2}{r^3} (\delta_{pq} - 3n_p n_q) g_p g_q, \quad (4)$$

$$K_{pq}^{\text{Ex}} = \left(\frac{g_{pq}}{g_J} \right)^2 (g_J - 1)^2 j, \quad (5)$$

where r is the interionic distance; n_k is the directional cosines of the line connecting the ions; p and q are x, y, z ; g_J is the Lande factor and j is the constant of isotropic exchange interaction.

Using Eq. (4), we have obtained that $K_{zz}^{\text{MDD}} = -0.1987 \text{ cm}^{-1}$ and $K_{zz}^{\text{Ex}} = +0.2715 \text{ cm}^{-1}$. From Eq. (5), it results that the value of isotropic exchange interaction of $j = +0.025 \text{ cm}^{-1}$ is 2.4 times less than the exchange

interaction for the dysprosium ions in similar crystal lattice [16].

Thus, the analysis of EPR spectrum and estimation of SSI allow to conclude that in the crystal investigated, the exchange interaction exceeds the magnetic dipole–dipole interaction and has an opposite sign. Such character of spin–spin interactions should lead to an antiferromagnetic ordering of $\text{RbNd}(\text{WO}_4)_2$ at low temperatures.

Acknowledgments

This work was supported in part by the EU project DT-CRYS and by Polish State Committee on Science (KBN) (decision of project no. 72/E-67/SPB/6. PR/DIE 430/2004-2006).

References

- [1] A.A. Kaminskii, A.F. Konstantinova, V.P. Orekhova, A.V. Butashin, R.F. Klevtsova, A.A. Pavlyuk, *Kristallografija* 46 (2001) 733 (*Sov. Phys. Crystallogr.*); X. Mateos, M.C. Pujol, F. Guell, M. Galan, R.M. Sole, J. Gavalda, M. Aguilo, J. Massons, F. Diaz, *IEEE Journal of Quantum Electronics* 40 (2004) 759.
- [2] M.T. Borowiec, V. Dyakonov, A. Jedrzejczak, V. Markovich, A. Pavluk, H. Szymczak, E. Zubov, M. Zaleski, *Phys. Lett. A* 243 (1998) 85; M.T. Borowiec, V. Dyakonov, V. Kamenev, A. Nabialek, A. Prokhorov, H. Szymczak, M. Zaleski, *Acta Phys. Pol. A* 94 (1998) 71.
- [3] M.T. Borowiec, Y.M. Kharchenko, T. Zayarnyuk, V.P. Dyakonov, M. Baranski, H. Szymczak, *J. Appl. Spectrosc.* 71 (2004) 651; M.T. Borowiec, A. Watterich, T. Zayarnyuk, V.P. Dyakonov, A. Majchrowski, J. Zmija, M. Baranski, H. Szymczak, *J. Appl. Spectrosc.* 71 (2004) 810.
- [4] M.T. Borowiec, V. Dyakonov, S. Piechota, A. Prokhorov, H. Szymczak, *Physica B* 240 (1977) 21.
- [5] P.V. Klevtsov, L.P. Kozeeva, R.F. Klevtsova, *Izv. Akad. Nauk SSSR Ser. Neorg. Mater.* 4 (1968) 1147.
- [6] S.V. Borisov, R.F. Klevtsova, *Kristallografija* 13 (1968) 517 (*Sov. Phys. Crystallogr.* 13 (1968)).
- [7] J.K. Viscakas, I.V. Mochalov, A.V. Mikhailov, R.F. Klevtsova, A.V. Lyubimov, *Litov. Fiz. Sbor.* 28 (1988) 224 (*Lithua. Phys. Collect.* 28 (1988)).
- [8] C. Zaldo, M. Rico, C. Cascales, M.C. Pujol, J. Massons, M. Aguilo, F. Diaz, P. Porcher, *J. Phys.: Condens. Matter* 12 (2000) 8531.
- [9] L. Masalik, J. Hanuza, B. Masalik, W. Ryba-Romanowski, S. Golab, A. Pietraszko, *J. Lumin.* 79 (1998) 9.
- [10] M.C. Pujol, M. Rico, C. Zaldo, R. Sole, V. Nikolov, X. Solans, M. Aguilo, F. Diaz, *Appl. Phys. B* 68 (1999) 187.
- [11] K. Kirshbaum, A. Martin, A.A. Pinkerton, *J. Appl. Cryst.* 30 (1997) 514.
- [12] G.M. Sheldrick, *Acta Crystallogr. A* 46 (1990) 467.
- [13] G.M. Sheldrick, *SHELXL93*, Program for the Refinement of Crystal Structures, University of Göttingen, Germany.
- [14] *International Tables for Crystallography*, edited by A.J.C. Wilson, Kluwer Press, Dordrecht, 1992.
- [15] M.T. Borowiec, V. Dyakonov, A. Prokhorov, H. Szymczak, *Phys. Rev. B* 62 (2000) 5834.
- [16] I.M. Krygin, A. Prokhorov, V. Dyakonov, M.T. Borowiec, H. Szymczak, *Sov. Phys. Solid State* 44 (2002) 1587.
- [17] I.M. Krygin, A.D. Prokhorov, *ZhETF* 92 (1987) 549 (*Sov.: JETP* 92 (1987)).
- [18] A. Abragam, B. Bleaney, *Electron Paramagnetic Resonance of Transition Ions*, vol. 1, Clarendon Press, Oxford, 1970.